Am J Transl Res 2026;18(1):91-111
www.ajtr.org /ISSN:1943-8141/AJTR0169419

Original Article

Integrated single-cell analysis with experimental validation reveals ANXA2 as a therapeutic target for ferroptosis in inflammatory bowel disease

Houshu Tu[1], Menglin Chen[1], Panpan Zhu[2], Ling He[4], Jing Hong[3]

[1]School of Clinical Medicine, Jiangxi University of Traditional Chinese Medicine, Nanchang 330004, Jiangxi, China; [2]Gyong Huang School of Traditional Chinese Medicine, Jiangxi University of Traditional Chinese Medicine, Nanchang 330004, Jiangxi, China; [3]Otolaryngology Department, Affiliated Hospital of Jiangxi University of Traditional Chinese Medicine, Nanchang 330006, Jiangxi, China; [4]Gastroenterology Department, Affiliated Hospital of Jiangxi University of Traditional Chinese Medicine, Nanchang 330006, Jiangxi, China

Received October 19, 2025; Accepted December 16, 2025; Epub January 15, 2026; Published January 30, 2026

Abstract: Background: Inflammatory bowel disease (IBD) is a chronic inflammatory disease characterized by intestinal dysfunction. Ferroptosis is a critical pathogenic mechanism in IBD. However, the therapeutic targets for ferroptosis-related IBD progression remain unclear. Therefore, this study aimed to identify potential therapeutic targets associated with ferroptosis in IBD. Methods: Single-cell RNA sequencing data (GSE134809) were analyzed using gene set scoring, cell-cell communication, pseudotime analysis, and high-dimensional gene co-expression network analysis (hdWGCNA) to screen for ferroptosis-related targets. *In vitro* experiments, including RT-qPCR, western blotting, flow cytometry, and ELISA, were performed to verify the regulatory role of annexin A2 (ANXA2) in ferroptosis and inflammation using its silencing or overexpression. For *in vivo* validation, a dextran sulfate sodium (DSS)-induced IBD mouse model was established. Immunofluorescence (IF) staining was then performed to examine ANXA2 expression and its co-localization with collagen type I alpha 2 chain (COL1A2) and 4-hydroxynonenal (4-HNE) in colon tissues. Results: Bioinformatic analysis of 28,974 cells identified that fibroblasts, particularly the Fibro_2 subpopulation, were highly associated with ferroptosis, with ANXA2 identified as a core target. *In vitro*, ANXA2 silencing significantly inhibited ferroptosis, oxidative stress, and inflammatory factors interleukin-6 (IL-6) and C-X-C Motif Chemokine Ligand 8 (CXCL8), whereas ANXA2 overexpression demonstrated the opposite effects. *In vivo*, ANXA2 was significantly up-regulated in the colon tissues of IBD mice, showing strong co-localization with the fibroblast marker COL1A2 and the ferroptosis marker 4-HNE. Conclusion: ANXA2 is highly expressed in fibroblasts and is associated with the ferroptosis of IBD, providing a novel therapeutic target for treatment of IBD.

Keywords: Inflammatory bowel disease, ANXA2, single-cell transcriptomics, ferroptosis

Introduction

Inflammatory bowel disease (IBD) is a chronic inflammatory gastrointestinal disease that seriously affects human health. It primarily includes ulcerative colitis and Crohn's disease, which are autoimmune diseases [1]. Clinically, IBD patients usually present with vomiting, abdominal pain, diarrhea, and bloody stool; and in severe cases, intestinal perforation, intestinal obstruction, and carcinogenesis may occur [2]. In recent years, the morbidity of IBD has been increasing. It is listed as a modern refractory disease by the World Health Organization, affecting millions of people in the world [3]. Although the exact etiology of IBD remains unknown, increasing evidence suggests that individual genetic susceptibility, intestinal microbiota, immune response, and environmental factors are all involved in the pathogenesis of IBD [4]. Currently, aminosalicylic acid, thiopurines, corticosteroids, biological agents, and immunosuppressants are primarily used for the clinical treatment of IBD [5]. While these treatments are effective in inducing remission in patients with mild disease, their efficacy in severe IBD is limited, and their long-term use is frequently associated with adverse reactions,

https://doi.org/10.62347/IQQX1658

including anorexia and osteoporosis [6, 7]. Therefore, identifying novel therapeutic targets for IBD remains an urgent clinical need.

Annexin A2 (ANXA2), a type of calcium-dependent protein that specifically binds to phospholipids, mainly expresses on the surface of endothelial cells and tumor cells. It participates in membrane related events, such as membrane aggregation, fusion, and formation to regulate multiple cellular functions, including cell proliferation, apoptosis, invasion and migration [8, 9]. A previous study demonstrated that ANXA2 regulates the intestinal cytoskeleton and affects tight junctions between intestinal cells by binding to F-actin in intestinal cells [10]. Moreover, ANXA2 was reported to be upregulated in migrated intestinal mucosal epithelial cells and to promote intestinal epithelial wound closure by modulating the small GTPase RhoA [11]. In addition, the depletion of ANXA2 was proven to improve intestinal inflammation by inhibiting the cleavage of TNF-α and induce cell proliferation and mucosal repair by promoting the cleavage of AREG and HB-EGF [12]. Although these studies had suggested a role of ANXA2 in intestinal homeostasis, its specific functions and related mechanisms of ANXA2 in IBD remain largely unclear.

Ferroptosis, a novel cell death form that is distinct from apoptosis and necrosis, is characterized by iron dependence and lipid peroxidation [13]. Previous research suggested that IBD could cause iron deficiency anemia due to malabsorption, and oral administration of iron has been used clinically to treat IBD-induced iron deficiency anemia [14]. However, intestinal iron overload can generates excessive reactive oxygen species (ROS) through the Fenton reaction that disrupt the gut microbiota [15]. The sustained oxidative stress state induces lipid peroxidation and stimulates secretion of inflammatory cytokines, further disrupting intestinal mucosal homeostasis and exacerbating inflammatory response in IBD [16]. Recently, numerous studies have demonstrated that iron chelators can promote the growth of beneficial gut microbiota, thereby protecting the intestinal mucosa and alleviating chronic intestinal inflammation [17, 18]. In addition, computational analyses have identified ANXA2 as a ferroptosis-related gene and a possible diagnostic biomarker for non-alcoholic fatty liver disease [19]. Meanwhile, experimental results further indicated the positive relationship between ANXA2 and ferroptosis in severe acute pancreatitis [20]. However, it is still unclear whether ANXA2 is associated with ferroptosis in IBD.

Based on the above background, this study employed single-cell transcriptomics to determine whether ANXA2 is a ferroptosis-related gene in IBD, and further investigated whether ANXA2 is highly expressed in the fibroblasts and predominantly associated with ferroptosis in IBD *in vivo*, thereby providing a novel target for the clinical treatment of IBD.

Materials and methods

Acquisition and processing of single-cell RNA sequencing (scRNA-seq) data

The scRNA-seq data, GSE134809, were downloaded from the National Genome Sequence Archive (https://ngdc.cncb.ac.cn/gsa/). The dataset includes samples from both lesional and non-lesional sites of 11 IBD patients. After being processed by the *Seurat* software package (v.4.3.0), the percentage of mitochondria and rRNA were calculated using the *PercentageEigenSet* function. Cells with fewer than 200 or more than 6000 detected genes, cells with mitochondrial gene expression exceeding 30%, and cells with fewer than 200 unique molecular identifiers (UMIs) were excluded, leaving a total of 28974 cells retained for subsequent analyses.

Annotation of scRNA-seq data

After standardization and normalization, principal component analysis (PCA) was used for dimensionality reduction of scRNA-seq data. Subsequently, the *FindAllMarkers* function in the *Seurat* software package was used to identify marker genes for each cell subpopulation. Finally, cell subpopulations were annotated to reveal their functional differences and development process using *SingleR* tool. The processed scRNA-seq data were mapped into a two-dimensional space to visually display the similarities and differences between cells by using the t-distributed stochastic neighbor embedding (t-SNE) algorithm. The highly expressed genes of each cell subpopulation were displayed in the form of bubble chart.

Gene set scoring

According to previous studies, the AUCell, single-sample gene set enrichment analysis (ssGSEA), UCell, AddModuleScore, singscore were performed based on single-cell gene expression ranking and the FerrDB database to score the ferroptosis-related gene set in this study [21-24]. After scoring, Student's t-test was used to analyze the significance of the ferroptosis-related gene set scores among different cell subpopulations between lesional and non-lesional sites in IBD patients.

Cell-cell communication analysis

According to the scoring results mentioned above, the cell subpopulations of the lesional site of IBD patients were further divided into two groups to explore the cell-cell communication, including the aggre_low and aggre_high groups, which respectively represented the cell subpopulation with low- and high-score of the ferroptosis-related gene set. After that, the *CellChat R* package was used to analyze the cell-cell communication based on the expression levels of ligands and receptors across different cell subpopulations. In short, after the "*identifyOverExpressedGenes*" and "*identifyOverExpressedInteractions*" functions were adopted to find highly expressed genes and pathways, the "*computeCommonProb*" function was used to calculate the number and strength of intercellular communication. The "*netAnalysis_signalingRole*" function was adopted to identify the sender (expression ligand) and receiver (expression receptor) in cell communication.

GESA enrichment analysis

According to the cell-cell communication results, fibroblasts were further selected for subsequent studies. In this study, gene set enrichment analysis (GSEA) was used to investigate the molecular mechanism associated with core genes in fibroblasts. In brief, after setting the permutation frequency to 1000 and the permutation type to phenotype, the ClusterProfiler tool was used for GESA based on gene sets from the Molecular Signatures Database (MSigDB).

Pseudotime analysis

The "*Monocle2*" package was used for pseudotime analysis of fibroblasts. In short, after extracting the expression matrix, gene information, and cell phenotype of fibroblasts, genes expressed in fewer than 10 cells were removed, and the top 1000 differentially expressed genes (DEGs) were then selected to construct the cell trajectory. Finally, the "DDRTree" algorithm was used for the dimensionality reduction of data.

High dimensional gene co-expression network analysis (hdWGCNA)

The "*hdWGCNA*" R package was used to construct gene co-expression networks, identify gene modules highly correlated with fibroblasts, and calculate the eigengene-based connectivity of modules. Finally, the *ModuleFeaturePlot* function was used to visualize each co-expression module.

Animals, animal experiment protocol, and establishing an IBD model

C57BL/6 male mice (n = 6, 7-week-old, 19-23 g) were purchased from Sinostem Biotechnology Co., Ltd. and acclimated for two weeks under standard conditions with ad libitum access to food and water and a 12 h light-dark cycle. All mice were randomly divided into two groups: the control and the IBD groups. Mice in the control group were conventionally fed, and the IBD model was established in mice of the IBD group. The IBD model of mice was established according to a previous study [25]. In short, mice received 1.5% dextran sulfate sodium salt (DSS, Lot., HY-116282, MedChemExpress, New Jersey, USA) dissolved in drinking water for one week and subsequently received normal drinking water for one week. IBD model was established after four cycles of DSS administration and normal water allowance. After the last cycle, the mice were euthanized by an intraperitoneal injection of an overdose of pentobarbital sodium (200 mg/kg). Death was confirmed by respiration and heartbeat cessation, as well as the absence of corneal reflex. Subsequently, the colon tissue was collected for subsequent studies. All animal experimental operations were approved by the Institutional Animal Care and Use Committee of Yi Shengyuan Gene Technology (Tianjin) Co., Ltd. (protocol number YSY-DWLL-2025732).

Immunofluorescence (IF) staining

IF staining was performed to determine ANXA2 expression and to evaluate its co-localization

Table 1. Primer sequence for RT-qPCR

Gene	Primer	Sequence (5'→e')
β-actin	Forward	CACCATTGGCAATGAGCGGTTC
	Reverse	AGGTCTTTGCGGATGTCCACGT
ANXA2	Forward	CCTCTTCACTCCAGCGTCATAG
	Reverse	TCGGACACATCTGGTGACTTCC

with fibroblasts, and ferroptosis-related markers in the colon tissue. The dissected colon tissues were fixed in 4% paraformaldehyde and embedded in paraffin. After deparaffinization, the tissues were sectioned into 2 μm-thick slices. All sections were subjected to antigen retrieval in EDTA buffer, incubated with 3% hydrogen peroxide solution for 25 minutes in the dark to block endogenous peroxidase activity, and then blocked with BSA for 30 minutes to reduce nonspecific binding. To determine ANXA2 expression and its co-localization with fibroblasts and ferroptosis-related markers in colon tissues, immunofluorescence staining was performed. Briefly, sections were incubated overnight at 4°C with an anti-ANXA2 antibody (1:200, Lot., ab189473), followed by incubation with a Cy3-labelled fluorescent secondary antibody for 50 minutes at room temperature. Tyramide signal amplification (TSA) was then applied for 10 minutes in the dark at room temperature, after which sections were subjected to a second round of antigen retrieval using EDTA buffer. After that, all sections were respectively incubated overnight at 4°C with collagen type I alpha 2 chain (COL1A2, 1:200, Lot., ab308455) and 4-hydroxynonenal (4-HNE, 1:300, Lot., ab48506) antibodies, followed by incubation with FITC-labeled fluorescent secondary antibody for 50 minutes at room temperature. All used antibodies were purchased from Abcam (Cambridge, UK). Finally, nuclei were counterstained with DAPI staining solution for 10 minutes in the dark at room temperature, followed by treatment with fluorescence quencher liquid B for 5 minutes. The co-localizations were observed and recorded using a fluorescence microscope.

Cell culture and transfection

The human normal colon fibroblast cell line (CCD-18Co) was purchased from Hefei Wanwu Biotechnology Co., Ltd. to validate the regulatory role of ANXA2 in ferroptosis. The cells were cultured in CCD-18Co Cell Complete Medium (Wanwu, Delf-27045). All cells were maintained at 37°C in a humidified incubator containing 5% CO_2. For transfection assays, the ANXA2 overexpression plasmid (oe-ANXA2), small interfering RNA targeting ANXA2 (si-ANXA2), and their respective negative controls (NC-ANXA2) were synthesized by GenePharma (Shanghai, China). After reaching a confluency at approximately 70-80%, CCD-18Co cells were transfected with above vectors using Lipofectamine 3000 (Invitrogen, USA).

RT-qPCR

To evaluate the expression of ANXA2, total RNA was extracted from the cells using Trizol reagent (Invitrogen, 15596026). Subsequently, reverse transcription was performed to synthesize cDNA using the PrimeScript™ RT Master Mix (Takara, RR036A). RT-qPCR was then conducted utilizing the TB Green® Premix Ex Taq™ II (Takara, RR820A) on a real-time PCR system. The specific primer sequences used in this study are listed in **Table 1**.

Western blot

Total protein was extracted from CCD-18Co cells using RIPA lysis buffer (Solarbio, R0010) and quantified with a BCA Protein Assay Kit (Thermo Fisher Scientific, 3225). Proteins were separated by 10-12% SDS-PAGE and transferred onto PVDF (Millipore, ISEQ00010). After blocking, the membranes were incubated overnight at 4°C with primary antibodies against ANXA2 (Abcam, ab189473), GPX4 (Abcam, ab125066), FTH1 (Abcam, ab183781), 4-HNE (Abcam, ab48506), and β-actin (Abcam, ab8227). Subsequently, the membranes were incubated with HRP-conjugated secondary antibodies (Abcam, ab6721) for 1 h. Protein bands were visualized using an ECL substrate (Thermo Fisher Scientific, 32106) and analyzed by ImageJ software.

Detection of lipid peroxidation

Lipid peroxidation, an indicator of ferroptosis, was determined using the C11-BODIPY 581/591 probe (Invitrogen, D3861). Transfected cells were incubated with 10 μM C11-BODIPY 581/591 probe for 30 min at 37°C, washed with PBS, and analyzed by flow cytometry (BD Biosciences). The extent of lipid peroxidation was quantified by measuring the mean

fluorescence intensity (MFI) of the oxidized probe.

ELISA and biochemical assays

To evaluate the regulation of ANXA2 on inflammatory cytokines and oxidative stress markers, commercial kits were used. Cell culture supernatants were collected to detect IL-6 (Elabscience, EH2IL6) and CXCL8 (Invitrogen, 88-8086-88) using ELISA kits. For oxidative stress assessment, cells were lysed using ultrasonication, and the levels of MDA and GSH were determined using biochemical assay kits (Nanjing Jiancheng Bioengineering Institute, A003-1-2; A005-1-2). The optical density (OD) values were measured using a microplate reader.

Statistical analysis

All data were obtained from at least three independent experiments and expressed as mean ± standard deviation. Statistical analyses were determined using Student's *t*-test with GraphPad Prism 8.0.2 (La Jolla, California, USA). A p-value < 0.05 was considered significant.

Results

Annotation of cell subpopulation and ferroptosis-related gene scoring

To explain transcriptome changes in different cell subpopulations of IBD, the GSE134809 dataset, containing the lesion and non-lesion sites in 11 IBD patients, was used in this study. After screening out 28974 cells using the "*Seurat*" package, PCA was then performed for dimensionality reduction, resulting in the identification of 25 distinct cell clusters (**Figure 1A**). Subsequently, based on the marker gene, all cell clusters were further annotated into 10 different cell subpopulations, including plasma B cells (marker genes: CD79A, CD37, CD19, CD79B, and MS4A1), dendritic cells (DC, marker genes: CD209), fibroblasts (marker genes: FGF7, MME, ACTA2, COL1A1, and COL3A1), endothelial cells (marker genes: PECAM1 and VWF), mast cells (marker genes: KIT and CPA3), monocytes (marker genes: CST3, LYZ, CD68, CD163, and CD14), T cells (marker genes: CD3D, CD3E, and CCR6), epithelial cells (marker genes: EPCAM, CDH1, CLDN4, KRT18, and KRT19), neutrophils (marker genes: CXCL8, NAMPT, and S100A8), and Paneth cells (marker genes: MMP7 and DEFA6) (**Figure 1B** and **1D**). Meanwhile, comparison of cell subpopulations between the lesional and non-lesional sites revealed marked alterations in immune cell composition at the lesional sites, characterized by an increased proportion of monocytes and a decreased proportion of dendritic cells, which is associated with the inflammatory pathology of IBD (**Figure 1C** and **1E**). Next, a total of 264 ferroptosis-related genes were identified from the FerrDB database, and ferroptosis activity was evaluated using AUCell, UCell, singscore, ssGSEA, and AddModuleScore algorithms. As illustrated in **Figure 1F**, the AUCell, UCell, singscore, ssGSEA, and AddModuleScore scoring and the total scoring were higher in the lesion (the I group) than those in the non-lesional site (the C group), indicating upregulated expression of ferroptosis-related genes in the IBD lesions. Furthermore, analysis of the ferroptosis-related gene scores across cell subpopulations demonstrated that plasma B cells, DC, fibroblasts, monocytes, T cells, epithelial cells, neutrophils, Paneth cells in the lesional site (the I group) exhibited higher ferroptosis-related scores than that in the non-lesional site (the C group) (**Figure 1G** and **1H**).

Cell-cell communication

To investigate further which cell subpopulation plays an essential role in the ferroptosis of IBD, the cells from lesional sites were stratified into two groups, namely, the aggre_low (with low ferroptosis-related gene score) and aggre_high groups (with high ferroptosis-related gene score). Cell-cell communication analysis was performed. As presented in **Figure 2A**, fibroblasts and Paneth cells displayed a larger interaction number and stronger interaction strength, indicating that these two kinds of cells played an essential role in the ferroptosis of IBD. In addition, further analysis found that the communication strength of 37 signaling pathways was significantly increased in the aggre_high group (marked in red) and the communication strength of 5 signaling pathways was significantly increased in the aggre_low group (marked in blue) (**Figure 2B**). Meanwhile, the comparison of incoming and outgoing interaction strength of different cell subpopulations in the aggre_low and aggre_high groups

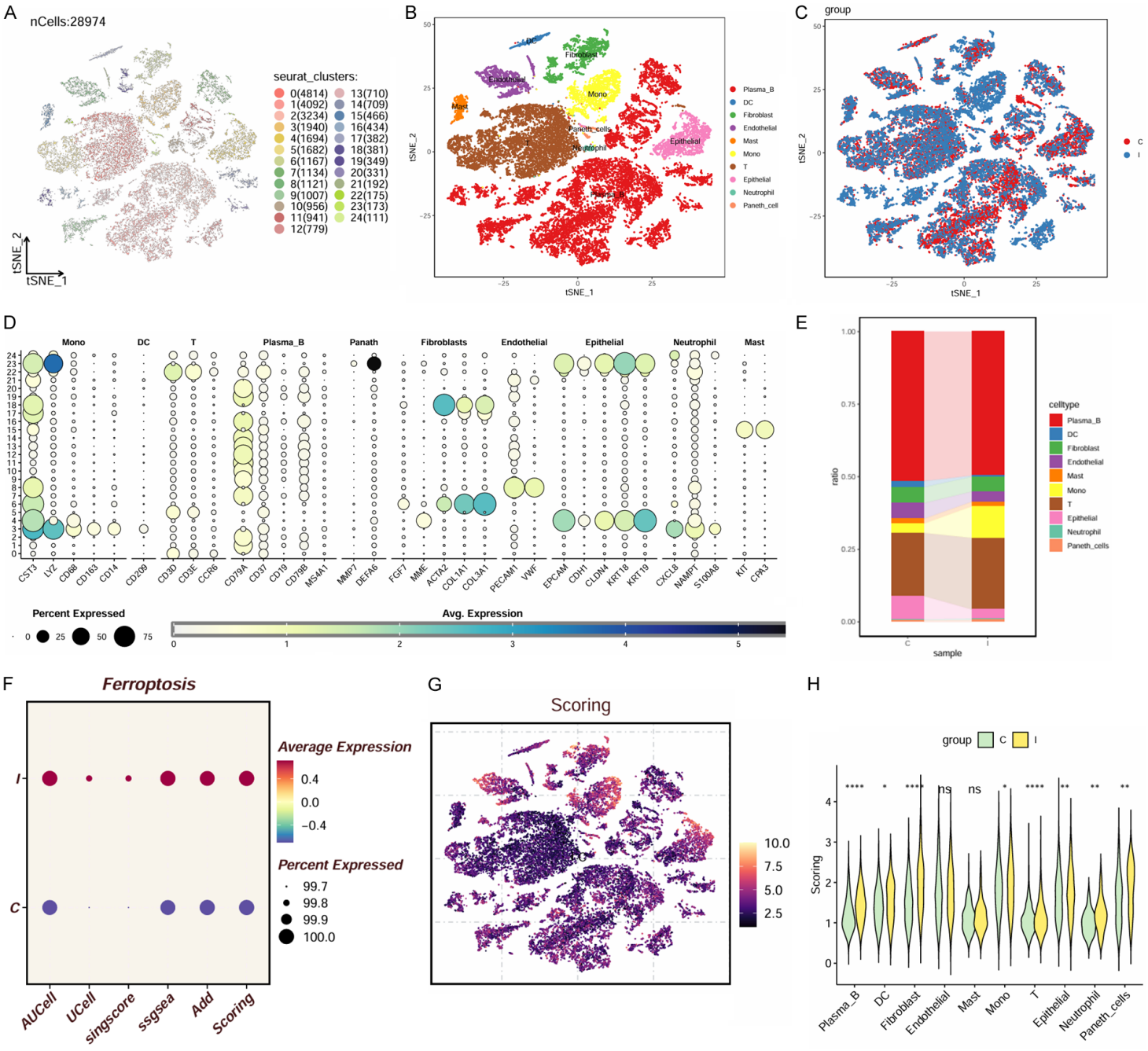
A
nCells:28974
seurat_clusters:
0(4814) 1(4092) 2(3234) 3(1940) 4(1694) 5(1682) 6(1167) 7(1134) 8(1121) 9(1007) 10(956) 11(941) 12(779) 13(710) 14(709) 15(466) 16(434) 17(382) 18(381) 19(349) 20(331) 21(192) 22(175) 23(173) 24(111)
tSNE_2
tSNE_1
B
DC
Fibroblast
Endothelial
Mast
Mono
Paneth_cells
Neutrophil
Epithelial
T
Plasma_B
Plasma_B
DC
Fibroblast
Endothelial
Mast
Mono
T
Epithelial
Neutrophil
Paneth_cell
tSNE_2
tSNE_1
C
group
C
I
tSNE_2
tSNE_1
D
Mono
DC
T
Plasma_B
Panath
Fibroblasts
Endothelial
Epithelial
Neutrophil
Mast
CST3 LYZ CD68 CD163 CD14 CD209 CD3D CD3E CCR6 CD79A CD37 CD19 CD79B MS4A1 MMP7 DEFA6 FGF7 MME ACTA2 COL1A1 COL3A1 PECAM1 VWF EPCAM CDH1 CLDN4 KRT18 KRT19 CXCL8 NAMPT S100A8 KIT CPA3
Percent Expressed
0 25 50 75
Avg. Expression
0 1 2 3 4 5
E
ratio
celltype
Plasma_B
DC
Fibroblast
Endothelial
Mast
Mono
T
Epithelial
Neutrophil
Paneth_cells
C
I
sample
F
Ferroptosis
I
C
Average Expression
0.4
0.0
−0.4
Percent Expressed
99.7
99.8
99.9
100.0
AUCell UCell singscore ssgsea Add Scoring
G
Scoring
10.0
7.5
5.0
2.5
H
group C I
Scoring
**** * **** ns ns * **** ** ** **
Plasma_B DC Fibroblast Endothelial Mast Mono T Epithelial Neutrophil Paneth_cells

Figure 1. Annotation of different cell subpopulations and scoring of ferroptosis-related genes. A. Identification of 25 cell clusters by the t-SNE algorithm. B. Detailed annotation of different cell clusters. C. Distribution of cell clusters between the lesion (I group) and non-lesional sites (C group). D. Bubble diagram of marker genes of different cell clusters. E. Stacked histogram of the proportions of different cell types in the lesion (I group) and non-lesional sites (C group). F. AUCell, ssGSEA, UCell, AddModuleScore, and singscore scoring results comparing the lesional (I group) and non- lesional sites (C group). G. Ferroptosis-related gene scores across different cell subpopulations. H. Violin plots of ferroptosis-related gene scores across different cell subpopulations between the lesional (I group) and non-lesional sites (C group).

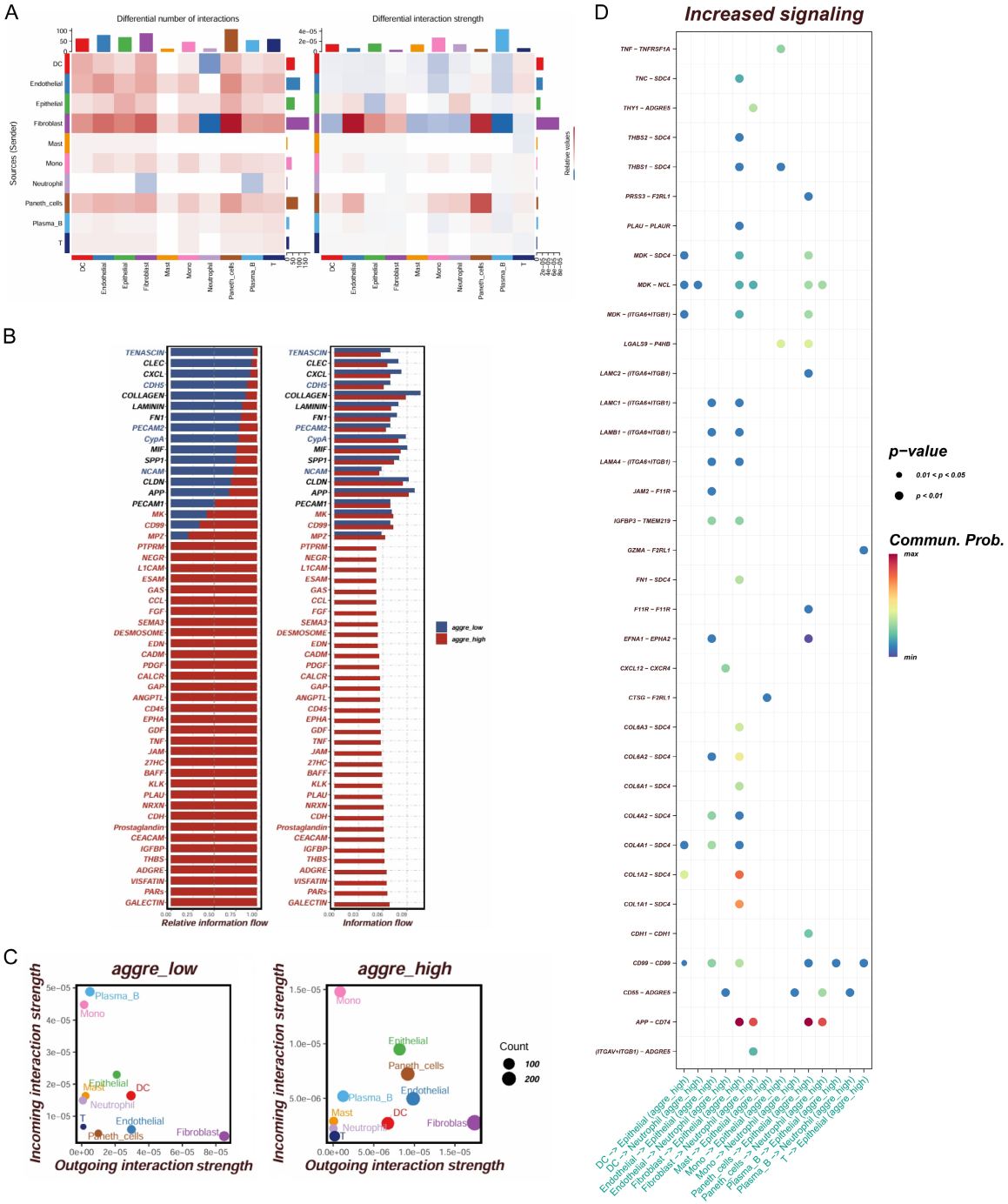

Figure 2. Cell-cell communication analysis. A. Heatmap of the interaction number and strength among different each cell subpopulations. B. Bar chart of the differences in enriched signaling pathways between the aggre_low

and aggre_high groups. C. Bubble chart of the incoming and outgoing interaction strength in the aggre_low and aggre_high groups. D. Scatter plot of increased ligand-receptor pairs among different cell subpopulations in the aggre_high group.

showed that fibroblasts possessed the strongest outgoing interaction strength in the aggre_low and aggre_high groups (**Figure 2C**). Finally, ligand-receptor interactions that increased among different cell subpopulations in the aggre_high group were analyzed. It was found that the APP-CD74 pair accounted for a large proportion of upregulated ligand-receptor interactions, and was predominantly associated with fibroblasts-epithelial cells, fibroblasts-neutrophils, Paneth cells-epithelial cells, and Paneth cells-neutrophils interactions (**Figure 2D**).

GSEA of fibroblasts

As the above results demonstrated that fibroblasts exhibited a larger interaction number, stronger interaction strength, and the largest outgoing interaction strength, fibroblast subpopulations in the lesion and non-lesion sites were further isolated for subsequent studies. After dimensionality reduction with PCA, fibroblast subpopulations in the lesional and non-lesional sites were further divided into seven cell subpopulations (**Figure 3A**). Comparison of fibroblast subpopulation proportions between lesional and non-lesional sites found that, compared to the non-lesional site (the C group), the proportions of Fibro_0, 1, 3, and 4 were reduced, while the proportions of Fibro_2 and 6 were elevated in the lesional site (the I group) (**Figure 3B**). The most significant change was observed in the proportion of Fibro_2, and therefore Fibro_2 cells were further compared between the lesional and non-lesional sites, with particular attention paid to the enrichment of associated pathways. The GSEA of the seven cell subpopulations in the lesion was performed. As illustrated in **Figure 3C**, different cell subpopulations were enriched in multiple pathways. The DEGs of the Fibro_2 cell subpopulation mainly included CCL11, ACTG2, MYL6, ACTA2, MYLK, IGFBP5, PDGFRRA, MT2A, COL1A1, CXCL8, CTHRC1, CTSK, CHI3L1, and SOD2. These DEGs of the Fibro_2 cell subpopulation were enriched in multiple pathways, including the “eosinophil chemotaxis”, “humoral immune response”, “eosinophil migration”, “complement activation”, “lymphocyte chemotaxis”, “muscle contraction”, “muscle system process”, “actin-mediated cell contraction”, “wound healing”, “cellular component assembly involved inmorphogenesis”, “platelet-derived growth factor receptor signaling pathway”, “muscle cell differentiation”, “glomerulus development”, “regulation of blood coagulation”, “regulation of hemostasis”, “response to copper ion”, “cellular response to zinc ion”, “response to metal ion”, “cellular response to copper ion”, “response to zinc ion”, “regulation of angiogenesis”, “regulation of vasculature development”, “regulation of inflammatory response”, “leukocyte chemotaxis”, “myeloid leukocyte migration”, “collagen metabolic process”, “collagen catabolic process”, “cellular response to UV-A”, and “extracellular matrix organization” pathways. In addition, the GSEA of the Fibro_2 cell subpopulation between the lesional and non-lesional sites was performed again. As presented in **Figure 3D** and **3E**, compared to the non-lesional site, the top three up-regulated pathways of Fibro_2 cell subpopulation in the lesion were “response to cytokine”, “response to abiotic stimulus”, and “anatomical structure morphogenesis” pathways, and the top three down-regulated pathways were “stem cell differentiation”, “oxidative phosphorylation”, and “aerobic respiration” pathways.

Pseudotime analysis of fibroblasts

As the above results demonstrated that the fibroblast subpopulations played an essential role in the ferroptosis of IBD, the differentiation capacity of fibroblasts was further analyzed. CytoTRACE was first used to predict the differentiation capacity of fibroblast subpopulations in the lesional and non-lesional sites, revealing significant differences between the two groups (**Figure 4A**). Moreover, comparison of CytoTRACE-predicted results with the phenotypes of fibroblast subpopulations in the lesional site showed that fibroblast subpopulations with high differentiative capacity was mostly enriched in the Fibro_2 cell subpopulation. The Fibro_5 cell subpopulation was identified as the developmental starting point, and the cell subpopulations were then divided into different

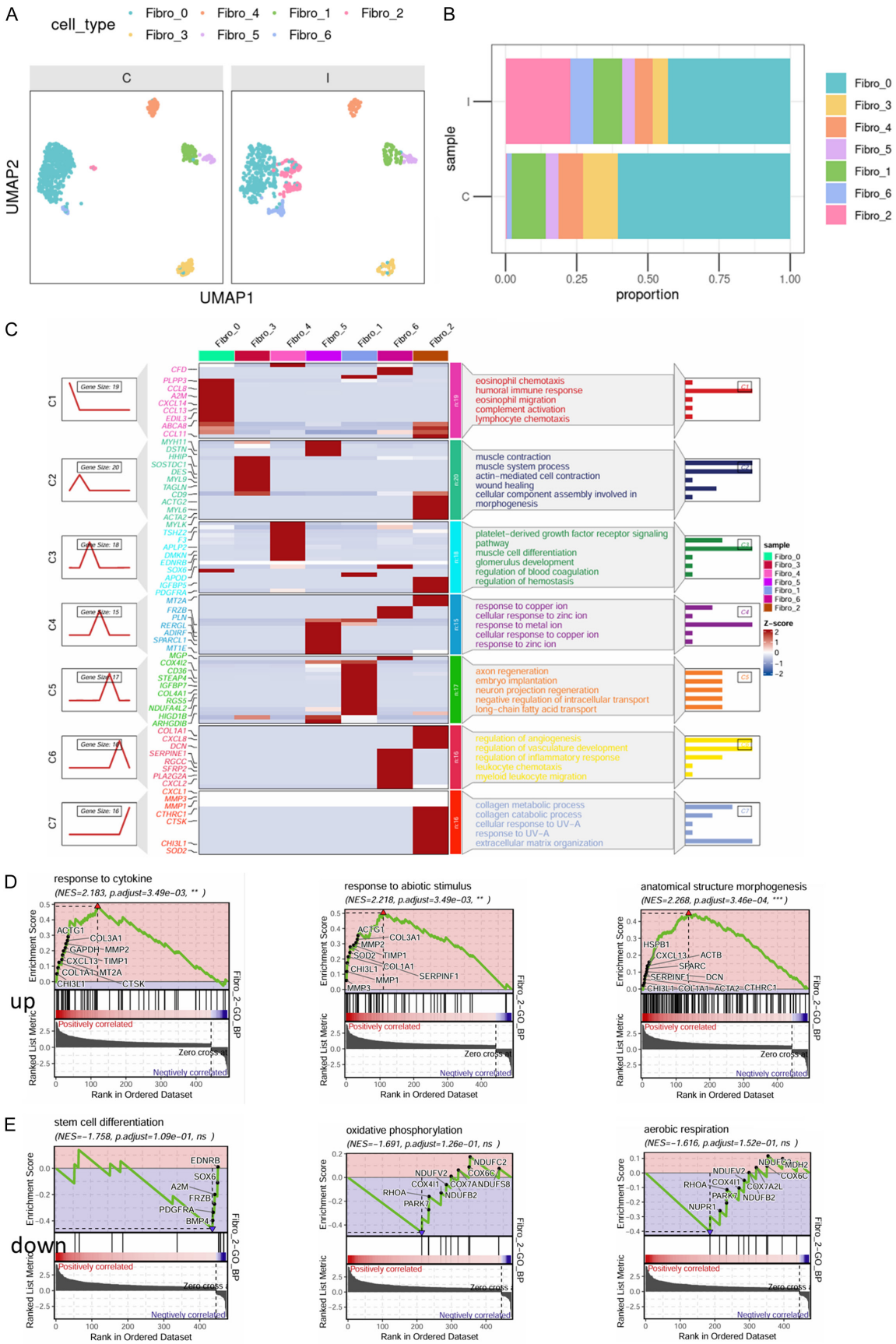
A
cell_type
Fibro_0
Fibro_4
Fibro_1
Fibro_2
Fibro_3
Fibro_5
Fibro_6
C
I
UMAP2
UMAP1
B
sample
proportion
C
C1
C2
C3
C4
C5
C6
C7
eosinophil chemotaxis
humoral immune response
eosinophil migration
complement activation
lymphocyte chemotaxis
muscle contraction
muscle system process
actin-mediated cell contraction
wound healing
cellular component assembly involved in morphogenesis
platelet-derived growth factor receptor signaling pathway
muscle cell differentiation
glomerulus development
regulation of blood coagulation
regulation of hemostasis
response to copper ion
cellular response to zinc ion
response to metal ion
cellular response to copper ion
response to zinc ion
axon regeneration
embryo implantation
neuron projection regeneration
negative regulation of intracellular transport
long-chain fatty acid transport
regulation of angiogenesis
regulation of vasculature development
regulation of inflammatory response
leukocyte chemotaxis
myeloid leukocyte migration
collagen metabolic process
collagen catabolic process
cellular response to UV-A
response to UV-A
extracellular matrix organization
sample
Z-score
D
response to cytokine
(NES=2.183, p.adjust=3.49e-03, **)
response to abiotic stimulus
(NES=2.218, p.adjust=3.49e-03, **)
anatomical structure morphogenesis
(NES=2.268, p.adjust=3.46e-04, ***)
up
Enrichment Score
Ranked List Metric
Rank in Ordered Dataset
Positively correlated
Negtively correlated
Zero cross
Fibro_2~GO_BP
E
stem cell differentiation
(NES=-1.758, p.adjust=1.09e-01, ns)
oxidative phosphorylation
(NES=-1.691, p.adjust=1.26e-01, ns)
aerobic respiration
(NES=-1.616, p.adjust=1.52e-01, ns)
down

Figure 3. GSEA of fibroblasts. A. UMAP plot of fibroblast subpopulations in the lesion (I group) and non-lesion sites (C group). B. Distribution of fibroblast subpopulations between the lesional (I group) and non-lesional sites (C group). C. GSEA of fibroblast subpopulations in the lesional site. D. Top three up-regulated pathways of the Fibro_2 cell subpopulation in the lesional site compared to the non- lesional site. E. Top three down-regulated pathways of the Fibro_2 cell subpopulation in the lesional site compared to the non- lesional site.

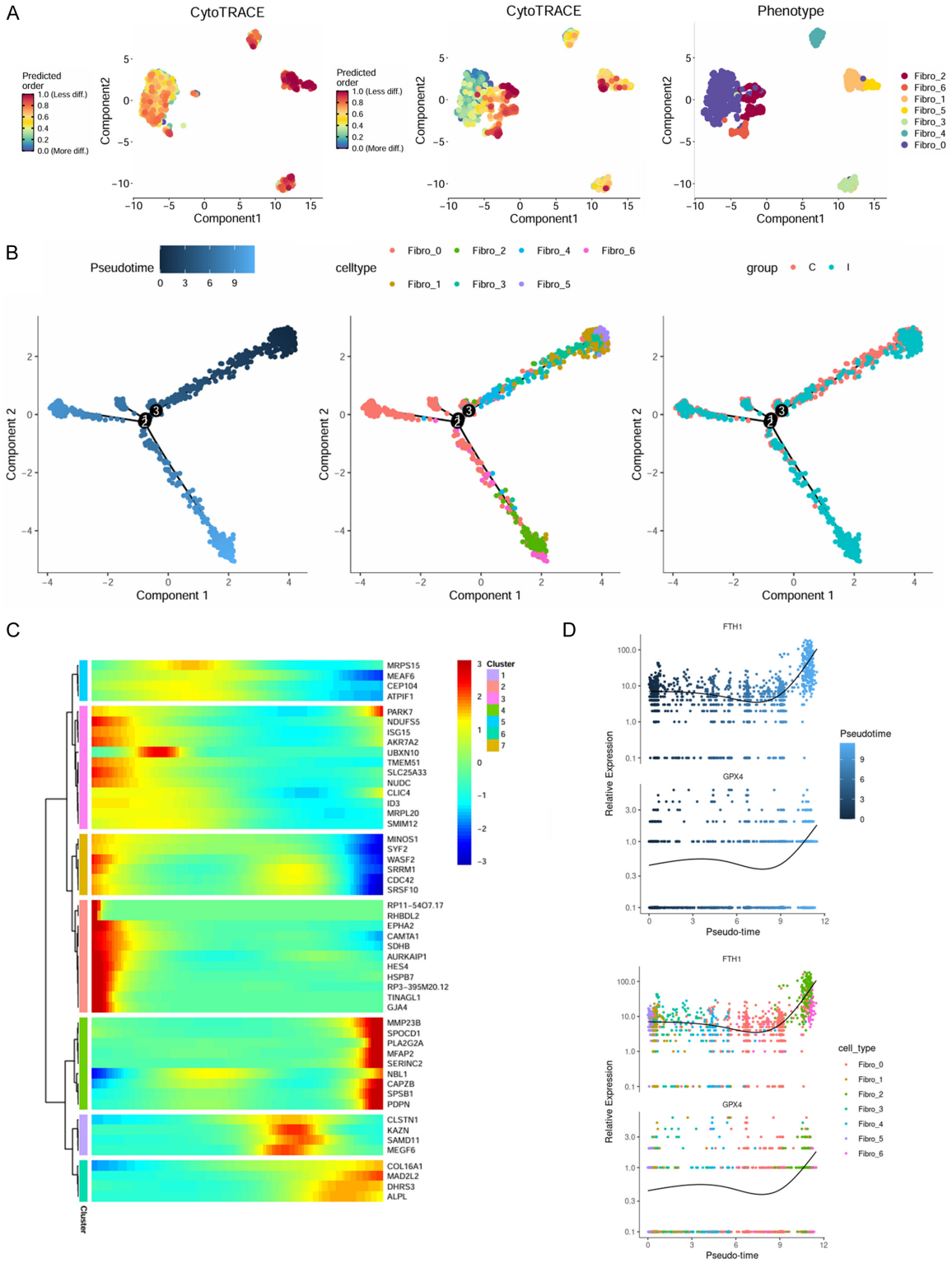

Figure 4. Pseudotime analysis of fibroblasts. A. Differentiation capacity of fibroblasts predicted by the CytoTRACE. B. Pseudotime analysis revealing the differentiation trajectory of fibroblasts. C. Heatmap of dynamic changes in gene expression across different cell clusters. D. Dynamic changes in FTH1 and GPX4 gene expression levels in different fibroblast subpopulations along pseudotime trajectory.

states according to branching points (**Figure 4B**). In addition, the trajectory of cell differentiation shifts from top to bottom over time, with Fibro_1, Fibro_3, and Fibro_5 cell subpopulations distributed in the early stage, Fibro_0 and Fibro_4 cell subpopulations roughly located in the intermediate stage, and Fibro_2 and Fibro_6 cell subpopulations distributed in the late stage of development. Moreover, the differences in the trajectory of fibroblast differentiation between the lesional site and the non-lesional site of IBD were mainly reflected in the early and late development stages. Then, the dynamic changes in gene expression of different cell clusters were analyzed. As presented in **Figure 4C**, the gene expression levels in the cluster 2, 3, 5, and 7 were gradually decreased with the development of the pseudotime and were gradually increased in cluster 1, 4, and 6. Meanwhile, with the development of the pseudotime, the relative expression levels of ferritin heavy chain 1 (FTH1) and glutathione peroxidase 4 (GPX4) were elevated, among which the enhancement of FTH1 expression level exceeded that of GPX4 (**Figure 4D**). Also, cells with high FTH1expression were mainly enriched in the Fibro_2 cell subpopulation at the late stage of differentiation.

hdWGCNA of fibroblasts

Subsequently, hdWGCNA was performed on fibroblasts to identify genes strongly associated with fibroblasts. It was found that the mean, median, and max connectivity were high and the scale-free network was more biologically significant when the soft power threshold was set to 1 (**Figure 5A**). Then, a hierarchical clustering tree was generated to group genes with similar expression patterns into different modules. A total of 10 modules were identified, which were distinguished using different colors (**Figure 5B**). Meanwhile, there was a strong correlation among different modules (**Figure 5C**). In addition, given the prominent role of the Fibro_2 cell subpopulation among fibroblasts, the correlation between different modules and fibroblast subpopulations was further analyzed. It showed that all modules were related to the Fibro_2 cell subpopulation, among which the Fibro_NEW10 module showed the strongest association (**Figure 5D**). Subsequently, the top 10 core genes in each module with high kME values were presented (**Figure 5E**). Given the strongest association between Fibro_NEW10 module with the Fibro_2 cell subpopulation, we paid special attention to the core genes in the Fibro_NEW10 module, identifying the top 10 core genes with high kME values in the Fibro_NEW10 module, including ANXA2, RHOA, TUBB, FIBIN, RARRES2, TMEM176B, MRGPRF, KDELR3, YWHAH, and KDELR2, among which ANXA2 possessed the highest kME value. Therefore, ANXA2 was considered as the potential therapeutic target associated with ferroptosis in IBD. Meanwhile, the *ModuleFeaturePlot* function was used to visualize the expression patterns of fibroblast subpopulation for the core gene with the highest kME value in each module (**Figure 5F**). As the Fibro_NEW10 module showed the strongest associated with the Fibro_2 cell subpopulation, the top 25 hub genes with the highest kME values in the Fibro_NEW10 module were further visualized (**Figure 5G**). Meanwhile, the top 25 hub genes across all modules were also visualized (**Figure 5H**). Finally, comparison of ANXA2 expression level revealed that the ANXA2 expression level in the lesional site was significantly higher than that in the non-lesional site of IBD ($P < 0.0001$, **Figure 5I**).

ANXA2 was highly expressed in fibroblasts and associated with the ferroptosis in IBD

As the above results suggested that ANXA2 may be a ferroptosis-related therapeutic target in IBD, we further determined ANXA2 expression and its co-localization with fibroblasts and ferroptosis-related markers in colon tissues from IBD mice. As presented in **Figure 6A**, compared to the control group, the proportion of ANXA2-positive cells in the colon tissues of the IBD group was significantly increased ($P < 0.0001$). Then, the colon tissues were counterstained with COL1A2 (fibroblast marker) and 4-HNE (ferroptosis marker) antibodies to determine the association between ANXA2 and fibroblasts as well as ferroptosis. As illustrated in **Figure 6B-H**, both the proportion of ANXA2-

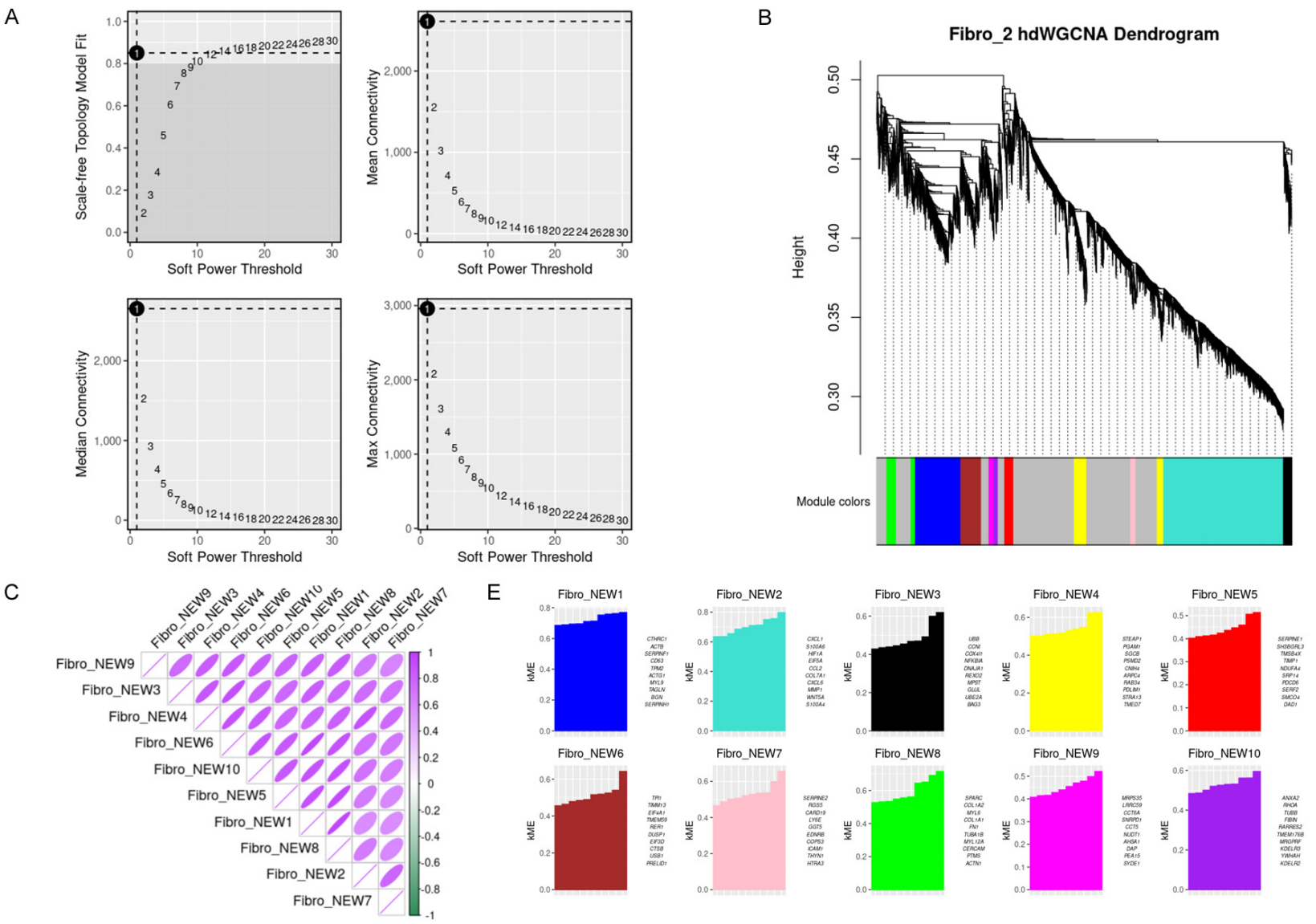
A
Scale-free Topology Model Fit
Soft Power Threshold
Mean Connectivity
Median Connectivity
Max Connectivity
B
Fibro_2 hdWGCNA Dendrogram
Height
Module colors
C
Fibro_NEW9
Fibro_NEW3
Fibro_NEW4
Fibro_NEW6
Fibro_NEW10
Fibro_NEW5
Fibro_NEW1
Fibro_NEW8
Fibro_NEW2
Fibro_NEW7
E
kME

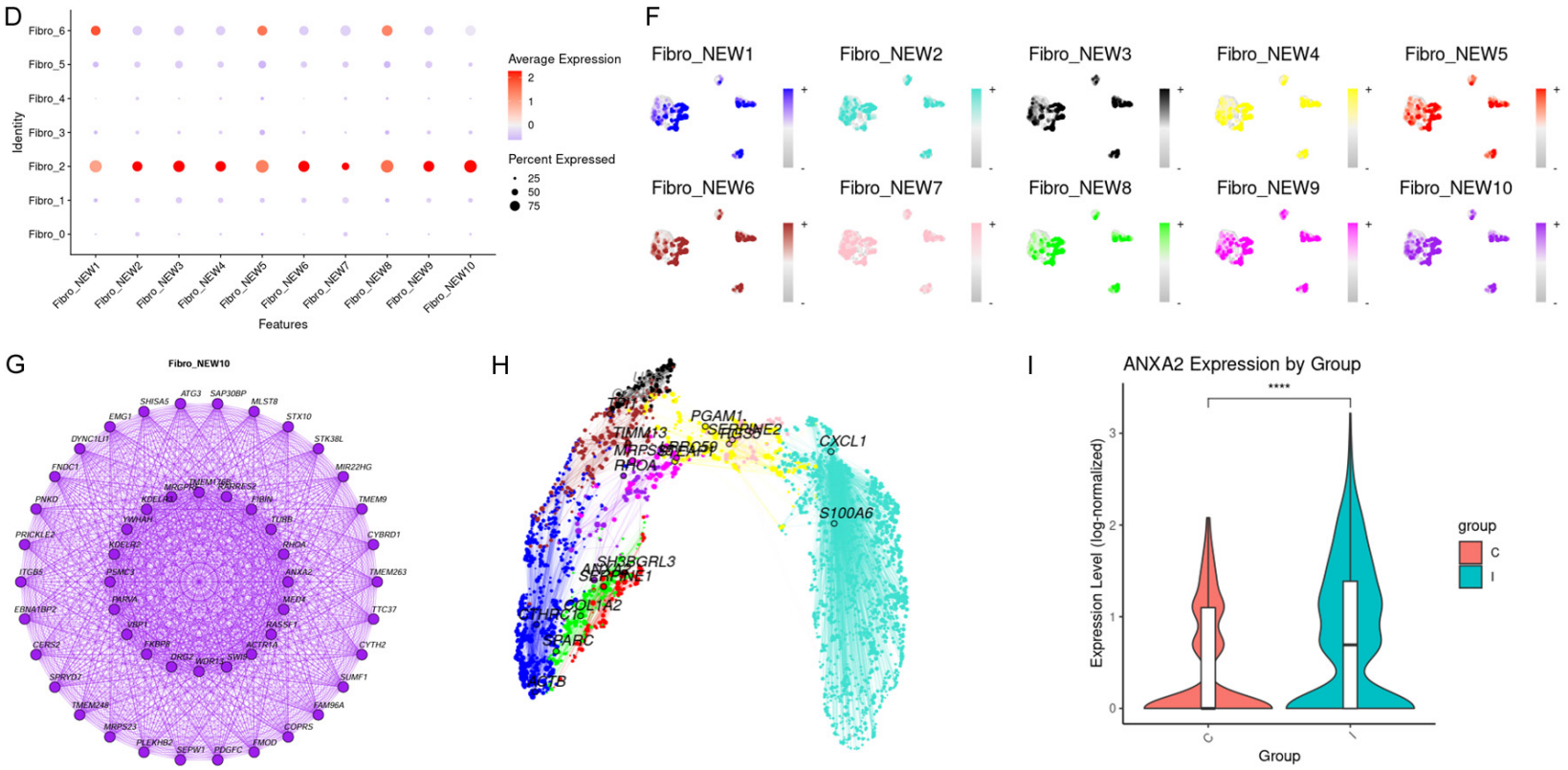

Figure 5. hdWGCNA of fibroblasts. A. Selection of the optimal soft-threshold power. B. Gene clustering tree diagram of fibroblasts. C. Correlation among different gene co-expression modules. D. Correlations between each module and fibroblast subpopulations. E. Core genes with high intramodular connectivity in each module based on kME values. F. Visualization of fibroblast subpopulations expressing the core gene with the highest kME value in each module. G. Top 25 hub genes in the Fibro_NEW10 module. H. Top 25 hub genes across all modules. I. Comparison of ANXA2 expression levels between the lesional (I group) and non- lesional sites (C group) of IBD. $^{****}P < 0.0001$ (Student's *t*-test).

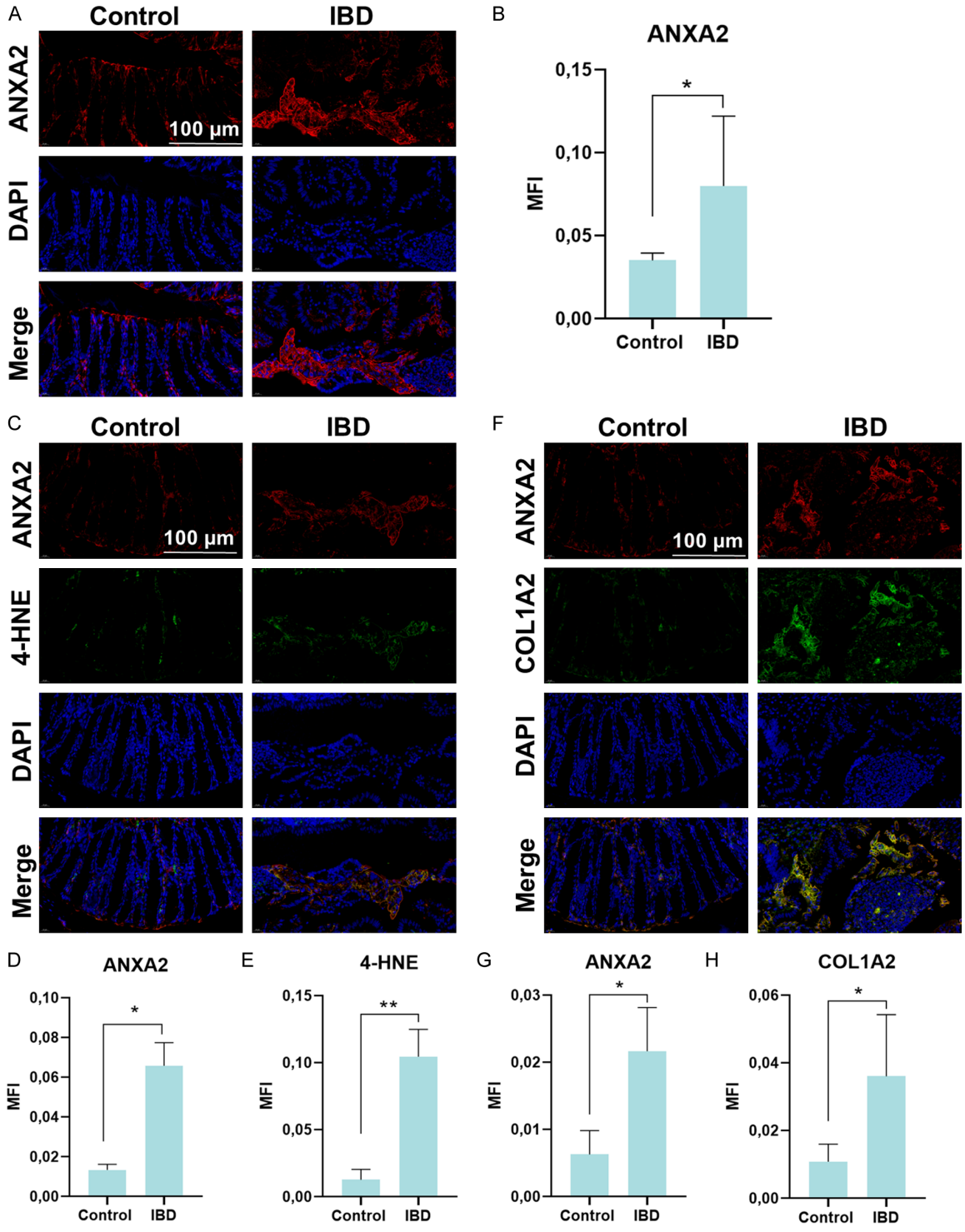

Figure 6. ANXA2 was highly expressed in fibroblasts and associated with the ferroptosis of IBD. (A, B) Evaluation of ANXA2 expression in colon tissues. Representative IF images showing ANXA2 (red) expression (A) and quantitative analysis of the mean fluorescence intensity (MFI) (B) in the Control and IBD groups. (C-E) Co-localization analysis of ANXA2 and the ferroptosis marker 4-HNE. Representative IF images displaying the co-localization of ANXA2 (red) and 4-HNE (green) (C). Quantitative analysis of the MFI of ANXA2 (D) and 4-HNE (E) corresponding to (C). (F-H) Co-localization analysis of ANXA2 and the fibroblast marker COL1A2. Representative IF images displaying the co-localization of ANXA2 (red) and COL1A2 (green) (F). Quantitative analysis of the MFI of ANXA2 (G) and COL1A2 (H) corresponding to (F). Nuclei were stained with DAPI (blue). Scale bar = 100 μm. Data are presented as mean ± SD (n = 3). *$P < 0.05$, **$P < 0.01$ vs. Control group.

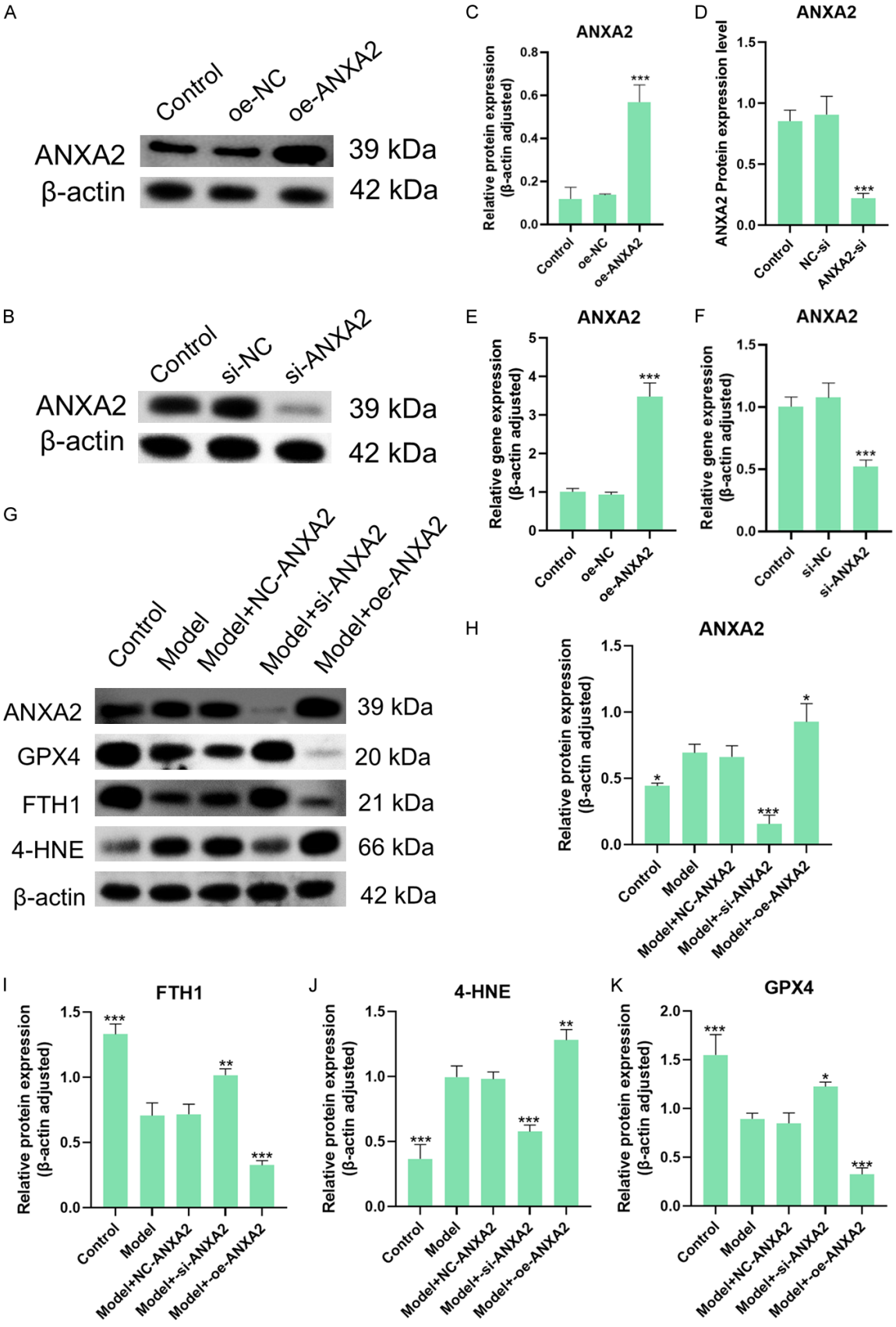
A
Control
oe-NC
oe-ANXA2
ANXA2
β-actin
39 kDa
42 kDa
B
Control
si-NC
si-ANXA2
ANXA2
β-actin
39 kDa
42 kDa
C
ANXA2
Relative protein expression (β-actin adjusted)
Control
oe-NC
oe-ANXA2
D
ANXA2
ANXA2 Protein expression level
Control
NC-si
ANXA2-si
E
ANXA2
Relative gene expression (β-actin adjusted)
Control
oe-NC
oe-ANXA2
F
ANXA2
Relative gene expression (β-actin adjusted)
Control
si-NC
si-ANXA2
G
Control
Model
Model+NC-ANXA2
Model+si-ANXA2
Model+oe-ANXA2
ANXA2
GPX4
FTH1
4-HNE
β-actin
39 kDa
20 kDa
21 kDa
66 kDa
42 kDa
H
ANXA2
Relative protein expression (β-actin adjusted)
Control
Model
Model+NC-ANXA2
Model+-si-ANXA2
Model+-oe-ANXA2
I
FTH1
Relative protein expression (β-actin adjusted)
J
4-HNE
Relative protein expression (β-actin adjusted)
K
GPX4
Relative protein expression (β-actin adjusted)

Figure 7. Validation of ANXA2 transfection efficiency and its regulatory effects on ferroptosis-related markers. (A, B) Representative western blot images showing ANXA2 overexpression (A) and silencing (B). The groups included Control, oe-NC, and oe-ANXA2 for overexpression, and Control, si-NC, and si-ANXA2 for silencing. (C, D) Quantitative analysis of ANXA2 protein levels corresponding to (A and B), respectively. (E, F) Relative mRNA expression of ANXA2 determined by RT-qPCR following transfection with overexpression (E) or silencing (F) constructs. (G) Representative western blot images of ANXA2, GPX4, FTH1, and 4-HNE proteins after modulation of ANXA2 expression. (H-K) Quantitative analysis of the protein levels of ANXA2 (H), FTH1 (I), 4-HNE (J), and GPX4 (K). Data are presented as mean ± SD. *$P < 0.05$, **$P < 0.01$, ***$P < 0.001$ vs. control group.

positive cells co-expressing COL1A2 or 4-HNE and the degree of co-localization were dramatically increased in the IBD group compared to that in the control group. These results indicate that ANXA2 is highly expressed in fibroblasts and is associated with ferroptosis in IBD.

ANXA2 regulated ferroptosis-related proteins

To further investigate the regulatory role of ANXA2 in ferroptosis, ANXA2 was silenced or overexpressed in fibroblast CCD-18Co cells. The transfection efficiency was verified using qPCR and Western blotting. The results showed that transfection with the ANXA2 overexpression plasmid significantly increased both the mRNA and protein levels of ANXA2 (**Figure 7A**, **7C**, **7E**). Conversely, ANXA2 silencing led to a significant reduction in its expression (**Figure 7B**, **7D**, **7F**). These results demonstrated that ANXA2 expression was successfully modulated in the cells.

Following this, we evaluated the effect of ANXA2 on the ferroptosis-related proteins GPX4 and FTH1, as well as the biomarker 4-HNE. We observed that ANXA2 silencing significantly decreased 4-HNE levels, whereas ANXA2 overexpression increased 4-HNE accumulation (**Figure 7G**, **7H**, **7J**). In contrast, GPX4 and FTH1, which act as negative regulators of ferroptosis, exhibited the opposite trend (**Figure 7I**, **7K**). These findings further indicate that ANXA2 promotes ferroptosis.

ANXA2 regulated ferroptosis levels and subsequent oxidative stress and inflammation

Following validation of the effects of ANXA2 on ferroptosis-related proteins, cell apoptosis was further assessed using flow cytometry to evaluate the regulatory role of ANXA2. The results showed that ANXA2 silencing significantly reduced apoptosis levels, whereas ANXA2 overexpression significantly increased it (**Figure 8A**, **8B**).

Given that ferroptosis is closely associated with oxidative stress and inflammation, oxidative stress markers MDA and GSH, as well as the inflammatory cytokines IL-6 and CXCL8 we subsequently examined. As expected, MDA (a marker of oxidative damage) and GSH (an antioxidant) exhibited opposite trends. Compared to the control group, ANXA2 silencing decreased MDA levels and increased GSH levels, while overexpression produced the opposite effects. Regarding inflammation, silencing ANXA2 reduced IL-6 and CXCL8 levels, whereas ANXA2 overexpression demonstrated a pro-inflammatory effect (**Figure 8C-F**).

Discussion

IBD is a chronic gastrointestinal inflammatory disease, commonly characterized by abdominal pain, diarrhea, and bloody stools [26]. Owing to its prolonged disease course, IBD is recognized as one of the risk factors for colitis and colorectal cancer, which not only greatly affects the quality of life of patients, but also imposes a heavy economic burden [27, 28]. At present, the mechanisms underlying IBD remain incompletely understood due to its complex pathogenesis. Therefore, it is necessary to further explore the pathogenesis of IBD, search for potential therapeutic targets, and provide more treatment options, which is beneficial for improving the prognosis and quality of life of IBD patients. Single-cell transcriptomic technology enables efficient and comprehensive characterization of cellular heterogeneity and diversity in tissues under pathological specific states, thereby identifying novel cell types and gene expression patterns involved in diseases occurrence and development [29]. Therefore, single-cell transcriptomic technology was used in this study to explore therapeutic targets of IBD.

Ferroptosis, a distinct form of cell death, not only regulates immune responses and promotes the release of inflammatory cytokines,

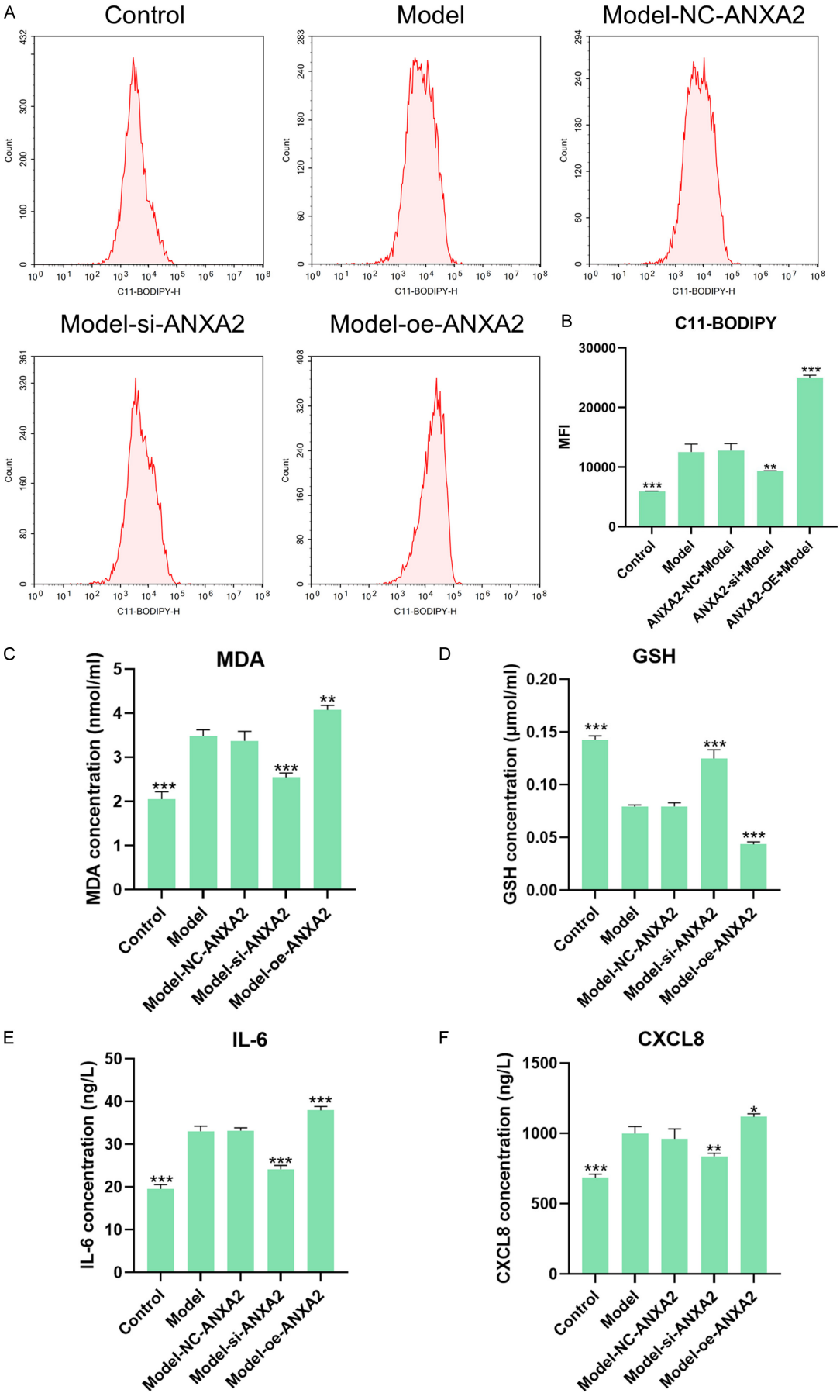
A
Control
Model
Model-NC-ANXA2
Model-si-ANXA2
Model-oe-ANXA2
Count
C11-BODIPY-H
B
C11-BODIPY
MFI
Control
Model
ANXA2-NC+Model
ANXA2-si+Model
ANXA2-OE+Model
C
MDA
MDA concentration (nmol/ml)
D
GSH
GSH concentration (μmol/ml)
E
IL-6
IL-6 concentration (ng/L)
F
CXCL8
CXCL8 concentration (ng/L)
Model-NC-ANXA2
Model-si-ANXA2
Model-oe-ANXA2

Figure 8. ANXA2 regulated ferroptosis-induced oxidative stress and inflammation. (A) Representative flow cytometry histograms showing lipid peroxidation levels (an indicator of ferroptosis) assessed using the C11-BODIPY 581/591 probe. (B) Quantitative analysis of the mean fluorescence intensity (MFI) of C11-BODIPY corresponding to (A). (C-F) Quantitative analysis of oxidative stress markers and inflammatory cytokines. The panels show the quantitative results for MDA (C), GSH (D), IL-6 (E), and CXCL8 (F). Data are presented as mean ± SD. $^{*}P < 0.05$, $^{**}P < 0.01$, $^{***}P < 0.001$ vs. control group.

but also participates in inflammatory processes by utilizing cyclooxygenase-related lipid peroxidation products [30]. In recent years, evidence has indicated that ferroptosis is also involved in the progression of IBD. A previous study indicated that excessive dietary iron altered gut phenotype, including the demethylation of quinone oxidoreductase 1 and glutathione peroxidase 2, to affect the iron-mediated intestinal diseases and regulate ferroptosis [31]. In addition, another study demonstrated that OTSSP167 effectively ameliorated IBD by inhibiting ferroptosis in the intestinal tissues and suppressing macrophage infiltration and M1 polarization to reduce the secretion of pro-inflammatory factors [32]. Therefore, in this study, after identifying and annotating all 10 different cell subpopulations, ferroptosis-related genes were scored across all cell subpopulations between the lesion site (I group) and the non-lesion site (C group). Our results suggested that the ferroptosis-related genes were highly expressed in the lesion site, with elevated scores observed in Plasma_B, DC, Fibroblast, Mono, T, Epithelial, Neutrophil, and Paneth_cell subpopulations. Further analysis demonstrated that fibroblasts and Paneth cells displayed higher numbers and strengths of intercellular interactions, with fibroblasts showing the strongest outgoing interaction strength, indicating that fibroblasts might be strongly associated with the ferroptosis of IBD.

Fibroblasts, an important component of the intestine, were previously believed to primarily play a role in tissue repair [33]. In recent years, increasing evidence has demonstrated that fibroblasts have multiple phenotypes, including inflammatory fibroblasts, myofibroblasts, and antigen-presenting fibroblasts [34]. These distinct fibroblast subsets might play an important role in the progression of IBD. Previous studies had shown that myofibroblasts are associated with the intestinal fibrosis of Crohn's disease [35]. Another study affirmed that inflammatory fibroblasts activated by bacterial antigens secreted inflammatory factors, such as IL-1β, to induce chemotaxis and activate intestinal immune cells [36]. In addition, one previous study profiling the expression of 940 genes in 1.35 million cells during the onset and recovery phases of experimental colitis revealed extensive crosstalk between fibroblasts and immune cells [37]. Therefore, based on the above results indicating that the fibroblasts might be strongly associated with ferroptosis of IBD, fibroblasts were extracted and divided into seven cell subpopulations for subsequent studies. Our studies found that the proportion of Fibro_2 in the lesion sites (I group) exhibited the most pronounced increase compared to the non-lesion sites (C group). Therefore, we further focused on the enriched DEGs and pathways of the Fibro_2 cell subpopulation. Our results indicated that the DEGs of the Fibro_2 cell subpopulation in the lesion site mainly included CCL11, ACTG2, MYL6, ACTA2, MYLK, IGFBP5, PDGFRRA, MT2A, COL1A1, CXCL8, CTHRC1, CTSK, CHI3L1, and SOD2; the top three up-regulated pathways of Fibro_2 cell subpopulation in the lesion site were "response to cytokine", "response to abiotic stimulus", and "anatomical structure morphogenesis" pathways, while the top three down-regulated pathways of Fibro_2 cell subpopulation in the lesion site were "stem cell differentiation", "oxidative phosphorylation", and "aerobic respiration" pathways. In addition, the results of pseudotime analysis of fibroblasts suggested that the Fibro_2 cell subpopulation distributed in the late stage of IBD development. Moreover, the pseudotime analysis results also indicated that cells with high FTH1 expression were mainly enriched in the Fibro_2 cell subpopulation during the late stage of development, hinting that the Fibro_2 cell subpopulation was associated with the ferroptosis of IBD. Finally, after the fibroblast subpopulations were further divided into 10 different modules according to similar expression pattern, the association between each module and each fibroblast subpopulation was analyzed. Our results suggested that the Fibro_NEW10 module demonstrated the strongest association with Fibro_2 cell subpopulation. Further analysis revealed that ANXA2 exhibited the highest kME value in the

Fibro_NEW10 module, which was considered as the potential ferroptosis-associated therapeutic target in IBD.

ANXA2, a member of the membrane-associated protein family, has been demonstrated to be associated with inflammatory responses [38]. A previous study demonstrated that the positive staining rate of ANXA2 in patients with ulcerative colitis (UC) was significantly upregulated compared to healthy control subjects, indicating that ANXA2 was closely associated with the pathogenesis of UC and may be a marker for differential diagnosis of IBD [39]. In addition, another study affirmed that ANXA2 was upregulated in mice with acute pancreatitis, which was positively related to the ferroptosis [20]. In this study, after predicting ANXA2 as the possible therapeutic target associated with ferroptosis in IBD, IF staining was performed to confirm the role of ANXA2 in the ferroptosis of IBD. Our results indicated that ANXA2 expression was significantly upregulated in the IBD group compared with the control group, which is consistent with previous reports. In addition, the co-localization of ANXA2 with COL1A2 and the ferroptosis marker 4-HNE was dramatically increased in the IBD group compared with that in the control group, suggesting that ANXA2 was highly expressed in fibroblasts and positively associated with the ferroptosis in IBD. However, a previous study affirmed that increased ANXA2 expression inhibited ferroptosis in pancreatic cancer, which was opposite to our results [40]. This discrepancy might be attributable to fundamental differences in genetic background, cellular context, and metabolic states between normal fibroblasts in inflammatory conditions and malignant tumor cells.

Despite these promising findings, several limitations of this study warrant further investigation. First, although we confirmed that ANXA2 regulates ferroptosis and inflammation in IBD using bioinformatic analysis, animal models, and cell experiments, the precise downstream molecular mechanisms remain incompletely understood. For instance, how ANXA2 interacts with or regulates the expression of GPX4 and FTH1 at the transcriptional or post-translational level requires further exploration. Second, while we utilized public single-cell datasets for human validation, this study lacks verification in a large-scale clinical cohort of IBD patients from our own center.

In the future, we will focus on delineating the specific signaling pathways mediated by ANXA2 in fibroblasts. Additionally, fresh clinical tissue samples will be collected to further validate the diagnostic and therapeutic value of ANXA2. Investigating small molecule inhibitors or neutralizing antibodies targeting ANXA2 may also provide a novel strategy for the clinical treatment of IBD.

Conclusions

A total of 28,974 cells from the GSE134809 dataset were divided into 25 clusters and 10 distinct cell subpopulations. Ferroptosis-related gene scores were significantly increased in the Plasma_B, DC, Fibroblast, Mono, T, Epithelial, Neutrophil, Paneth_cell subpopulations in IBD. Cell-cell communication analysis indicated that fibroblast cell subpopulation was closely associated with ferroptosis, involving multiple differently expressed genes and pathways. Pseudotime analysis suggested that the Fibro_2 cell subpopulation was associated with ferroptosis. The hdWGCNA identified ANXA2 as a potential target for ferroptosis in IBD. *In vivo*, ANXA2 was significantly up-regulated in the colon tissue of IBD mice and the co-localization of ANXA2 with COL1A2 and 4-HNE was also dramatically up-regulated in the colon tissues of IBD mice.

In conclusion, ANXA2 is highly expressed in fibroblasts and is associated with ferroptosis in IBD, providing a novel therapeutic target for the clinical treatment of IBD.

Acknowledgements

This study was supported by National Administration of Traditional Chinese Medicine (Project: Clinical Evidence-based Capacity Improvement for TCM Treatment of Advantageous Diseases) (Grant No. 2024-39).

Disclosure of conflict of interest

None.

Abbreviations

ANXA2, annexin A2; COL1A2, collagen type I alpha 2 chain; FTH1, ferritin heavy chain 1;

GPX4, glutathione peroxidase 4; hdWGCNA, high dimensional gene co-expression network analysis; IBD, inflammatory bowel disease; IF, immunofluorescence; PCA, principal component analysis; ssGSEA, single-sample gene set enrichment analysis; t-SNE, t-distributed stochastic neighbor embedding; UC, ulcerative colitis; 4-HNE, 4-hydroxynonenal.

Address correspondence to: Jing Hong, Otolaryngology Department, Affiliated Hospital of Jiangxi University of Traditional Chinese Medicine, 445 Bayi Avenue, Nanchang 330006, Jiangxi, China. E-mail: mnaaxtorerob1bijcp@163.com; Ling He, Gastroenterology Department, Affiliated Hospital of Jiangxi University of Traditional Chinese Medicine, Nanchang 330006, Jiangxi, China. E-mail: heling118@126.com

References

[1] Hodson R. Inflammatory bowel disease. Nature 2016; 540: S97.
[2] Gilliland A, Chan JJ, De Wolfe TJ, Yang H and Vallance BA. Pathobionts in inflammatory bowel disease: origins, underlying mechanisms, and implications for clinical care. Gastroenterology 2024; 166: 44-58.
[3] Ashton JJ and Beattie RM. Inflammatory bowel disease: Recent developments. Arch Dis Child 2024; 109: 370-376.
[4] Zhang YZ and Li YY. Inflammatory bowel disease: pathogenesis. World J Gastroenterol 2014; 20: 91-99.
[5] Pithadia AB and Jain S. Treatment of inflammatory bowel disease (IBD). Pharmacol Rep 2011; 63: 629-642.
[6] Wang M, Li R, Sheng S, Dong Z, Bai L, Wang X, Wang J, Lai Y, Chen X, Gao J, He C, Liu H and Su J. Combination therapy using intestinal organoids and their extracellular vesicles for inflammatory bowel disease complicated with osteoporosis. J Orthop Translat 2025; 53: 26-36.
[7] Ungaro RC, Kadali H, Zhang W, Adsul S and Reinisch W. Impact of concomitant 5-aminosalicylic acid therapy on vedolizumab efficacy and safety in inflammatory bowel disease: post hoc analyses of clinical trial data. J Crohns Colitis 2023; 17: 1949-1961.
[8] Illien F, Finet S, Lambert O and Ayala-Sanmartin J. Different molecular arrangements of the tetrameric annexin 2 modulate the size and dynamics of membrane aggregation. Biochim Biophys Acta 2010; 1798: 1790-1796.
[9] Sharma MC. Annexin A2 (ANX A2): an emerging biomarker and potential therapeutic target for aggressive cancers. Int J Cancer 2019; 144: 2074-2081.
[10] Xing R, He H, He Y, Feng Y, Zhang C, Wu H, Sun M, Yu X, Liu Y, Song X, Wang X, Chen Y and Hou Y. ANXA2 remodels the microstructures of caco2 cells. Cell Mol Biol (Noisy-le-grand) 2013; 59 Suppl: OL1848-1854.
[11] Babbin BA, Parkos CA, Mandell KJ, Winfree LM, Laur O, Ivanov AI and Nusrat A. Annexin 2 regulates intestinal epithelial cell spreading and wound closure through rho-related signaling. Am J Pathol 2007; 170: 951-966.
[12] Tanida S, Mizoshita T, Ozeki K, Katano T, Kataoka H, Kamiya T and Joh T. Advances in refractory ulcerative colitis treatment: a new therapeutic target, annexin A2. World J Gastroenterol 2015; 21: 8776-8786.
[13] Li J, Cao F, Yin HL, Huang ZJ, Lin ZT, Mao N, Sun B and Wang G. Ferroptosis: past, present and future. Cell Death Dis 2020; 11: 88.
[14] Mahadea D, Adamczewska E, Ratajczak AE, Rychter AM, Zawada A, Eder P, Dobrowolska A and Krela-Kaźmierczak I. Iron deficiency anemia in inflammatory bowel diseases - a narrative review. Nutrients 2021; 13: 4008.
[15] Lee T, Clavel T, Smirnov K, Schmidt A, Lagkouvardos I, Walker A, Lucio M, Michalke B, Schmitt-Kopplin P, Fedorak R and Haller D. Oral versus intravenous iron replacement therapy distinctly alters the gut microbiota and metabolome in patients with IBD. Gut 2017; 66: 863-871.
[16] Lee TW, Kolber MR, Fedorak RN and Van Zanten SV. Iron replacement therapy in inflammatory bowel disease patients with iron deficiency anemia: a systematic review and meta-analysis. J Crohns Colitis 2012; 6: 267-275.
[17] Wu Y, Ran L, Yang Y, Gao X, Peng M, Liu S, Sun L, Wan J, Wang Y, Yang K, Yin M and Chunyu W. Deferasirox alleviates DSS-induced ulcerative colitis in mice by inhibiting ferroptosis and improving intestinal microbiota. Life Sci 2023; 314: 121312.
[18] Chieppa M, Galleggiante V, Serino G, Massaro M and Santino A. Iron chelators dictate immune cells inflammatory ability: potential adjuvant therapy for IBD. Curr Pharm Des 2017; 23: 2289-2298.
[19] Qin J, Cao P, Ding X, Zeng Z, Deng L and Luo L. Machine learning identifies ferroptosis-related gene ANXA2 as potential diagnostic biomarkers for NAFLD. Front Endocrinol (Lausanne) 2023; 14: 1303426.
[20] He J, Hou X, Wu J, Wang K, Qi X, Wei Z, Sun Y, Wang C, Yao H and Liu K. Hspb1 protects against severe acute pancreatitis by attenuating apoptosis and ferroptosis via interacting with Anxa2 to restore the antioxidative activity of Prdx1. Int J Biol Sci 2024; 20: 1707-1728.
[21] De Cevins C, Delage L, Batignes M, Riller Q, Luka M, Remaury A, Sorin B, Fali T, Masson C,

Hoareau B, Meunier C, Parisot M, Zarhrate M, Pérot BP, García-Paredes V, Carbone F, Galliot L, Nal B, Pierre P, Canard L, Boussard C, Crickx E, Guillemot JC, Bader-Meunier B, Bélot A, Quartier P, Frémond ML, Neven B, Boldina G, Augé F, Alain F, Didier M, Rieux-Laucat F and Ménager MM. Single-cell RNA-sequencing of PBMCs from SAVI patients reveals disease-associated monocytes with elevated integrated stress response. Cell Rep Med 2023; 4: 101333.

[22] Subramanian A, Tamayo P, Mootha VK, Mukherjee S, Ebert BL, Gillette MA, Paulovich A, Pomeroy SL, Golub TR, Lander ES and Mesirov JP. Gene set enrichment analysis: a knowledge-based approach for interpreting genome-wide expression profiles. Proc Natl Acad Sci U S A 2005; 102: 15545-15550.

[23] Deng C, Deng G, Chu H, Chen S, Chen X, Li X, He Y, Sun C and Zhang C. Construction of a hypoxia-immune-related prognostic panel based on integrated single-cell and bulk RNA sequencing analyses in gastric cancer. Front Immunol 2023; 14: 1140328.

[24] Foroutan M, Bhuva DD, Lyu R, Horan K, Cursons J and Davis MJ. Single sample scoring of molecular phenotypes. BMC Bioinformatics 2018; 19: 404.

[25] Chen X, Liu G, Yuan Y, Wu G, Wang S and Yuan L. NEK7 interacts with NLRP3 to modulate the pyroptosis in inflammatory bowel disease via NF-κB signaling. Cell Death Dis 2019; 10: 906.

[26] Flynn S and Eisenstein S. Inflammatory bowel disease presentation and diagnosis. Surg Clin North Am 2019; 99: 1051-1062.

[27] Shah SC and Itzkowitz SH. Colorectal cancer in inflammatory bowel disease: mechanisms and management. Gastroenterology 2022; 162: 715-730, e3.

[28] Shahgoli VK, Noorolyai S, Ahmadpour Youshanlui M, Saeidi H, Nasiri H, Mansoori B, Holmskov U and Baradaran B. Inflammatory bowel disease, colitis, and cancer: unmasking the chronic inflammation link. Int J Colorectal Dis 2024; 39: 173.

[29] Aldridge S and Teichmann SA. Single cell transcriptomics comes of age. Nat Commun 2020; 11: 4307.

[30] Chen Y, Fang ZM, Yi X, Wei X and Jiang DS. The interaction between ferroptosis and inflammatory signaling pathways. Cell Death Dis 2023; 14: 205.

[31] Horniblow RD, Pathak P, Balacco DL, Acharjee A, Lles E, Gkoutos G, Beggs AD and Tselepis C. Iron-mediated epigenetic activation of NRF2 targets. J Nutr Biochem 2022; 101: 108929.

[32] Tang B, Zhu J, Fang S, Wang Y, Vinothkumar R, Li M, Weng Q, Zheng L, Yang Y, Qiu R, Xu M, Zhao Z and Ji J. Pharmacological inhibition of MELK restricts ferroptosis and the inflammatory response in colitis and colitis-propelled carcinogenesis. Free Radic Biol Med 2021; 172: 312-329.

[33] Chalkidi N, Paraskeva C and Koliaraki V. Fibroblasts in intestinal homeostasis, damage, and repair. Front Immunol 2022; 13: 924866.

[34] Tallquist MD. Cardiac fibroblast diversity. Annu Rev Physiol 2020; 82: 63-78.

[35] Bettenworth D, Bokemeyer A, Baker M, Mao R, Parker CE, Nguyen T, Ma C, Panés J, Rimola J, Fletcher JG, Jairath V, Feagan BG and Rieder F; Stenosis Therapy and Anti-Fibrotic Research (STAR) Consortium. Assessment of crohn's disease-associated small bowel strictures and fibrosis on cross-sectional imaging: a systematic review. Gut 2019; 68: 1115-1126.

[36] Neurath MF. Targeting immune cell circuits and trafficking in inflammatory bowel disease. Nat Immunol 2019; 20: 970-979.

[37] Cadinu P, Sivanathan KN, Misra A, Xu RJ, Mangani D, Yang E, Rone JM, Tooley K, Kye YC, Bod L, Geistlinger L, Lee T, Mertens RT, Ono N, Wang G, Sanmarco L, Quintana FJ, Anderson AC, Kuchroo VK, Moffitt JR and Nowarski R. Charting the cellular biogeography in colitis reveals fibroblast trajectories and coordinated spatial remodeling. Cell 2024; 187: 2010-2028, e30.

[38] Schmidinger B, Petri K, Lettl C, Li H, Namineni S, Ishikawa-Ankerhold H, Jiménez-Soto LF and Haas R. Helicobacter pylori binds human annexins via lipopolysaccharide to interfere with toll-like receptor 4 signaling. PLoS Pathog 2022; 18: e1010326.

[39] Zhang Z, Zhao X, Lv C, Li C and Zhi F. Annexin A2 expression in intestinal mucosa of patients with inflammatory bowel disease and its clinical implications. Nan Fang Yi Ke Da Xue Xue Bao 2012; 32: 1548-1552.

[40] Yang L, Wang R and Zhang L. HSPB1/KDM1 a facilitates ANXA2 expression via hypomethylated DNA promoter to inhibit ferroptosis and enhance gemcitabine resistance in pancreatic cancer. Naunyn Schmiedebergs Arch Pharmacol 2025; 398: 15665-15681.